Materials Science & Engineering A 657 (2016) 284–290

Contents lists available at ScienceDirect

Materials Science & Engineering A

journal homepage: www.elsevier.com/locate/msea

# Recrystallization, precipitation, and resultant mechanical properties of rolled Al–Zn alloy after aging

C.Y. Liu [a,b], B. Qu [a], Z.Y. Ma [c,*], M.Z. Ma [b], R.P. Liu [b]

[a] Key Laboratory of New Processing Technology for Nonferrous Metal & Materials, Ministry of Education, Guilin University of Technology, Guilin 541004, China
[b] State Key Laboratory of Metastable Materials Science and Technology, Yanshan University, Qinhuangdao 066004, China
[c] Shenyang National Laboratory for Materials Science, Institute of Metal Research, Chinese Academy of Sciences, 72 Wenhua Road, Shenyang 110016, China

ARTICLE INFO

*Article history:*
Received 14 December 2015
Received in revised form
22 January 2016
Accepted 25 January 2016
Available online 26 January 2016

*Keywords:*
Al–Zn alloy
Aging
Recrystallization
Precipitation
Mechanical properties

ABSTRACT

The recrystallization and precipitation behaviors of rolled Al–20 wt% Zn alloy were investigated during artificial aging. Recrystallization occurred preferentially in the shear bands, and recovery occurred in the elongated grains during aging at temperatures less than 200 °C. The aged Al–20 wt% Zn alloy showed a bimodal structure composed of fine grains and elongated coarse grains. The formation of Zn layers between Al grains, the coarsening of original Zn phase, and the precipitation of new Zn phase occurred at the same time during aging. The bimodal structure and thin Zn layers greatly affected the strengthening and deformation mechanisms of the Al–20 wt% Zn alloy. The aged Al–20 wt% Zn alloy showed the best mechanical properties after short-time aging at different aging temperatures.



## 1. Introduction

Deformation, such as high pressure torsion (HPT) [1–4], extrusion [4–6], rolling [7,8], accumulative roll bonding [9,10], and friction stir processing [11–13], has been widely used to improve the mechanical properties of metals. Most Al alloys show hardening after cold deformation because of grain refinement and dislocation increase through the Hall–Petch relationship and dislocation strengthening mechanism, respectively. However, recent papers have reported that the hardness of binary Al–Zn alloys significantly decreases with the increase in strain during HPT process [14–20].

Deformation has two competing effects on the strength of alloys: (i) hardening by grain refinement, increase of dislocations, and presence of nanosized precipitates; and (ii) softening by decomposition of supersaturated solid solution, coarsening of precipitates, coarsening of Al grains after completion of dynamic recrystallization, and annihilation of dislocations. Compared with solid solution-treated Al–Zn alloys (as-SS Al–Zn alloys), as-HPT Al–Zn alloys show finer Al grain size, low solubility in the Al matrix, and large number of precipitated Zn phase. The grain boundary (GB) hardening competes with softening because of the decomposition of supersaturated solid solution during deformation; the net effect is that HPT results in softening of Al–Zn alloys.

Aside from strain softening, other abnormal phenomena also occur in Al–Zn alloys after HPT. For example, Valiev et al. [16] found that as-HPT Al–30 wt%Zn alloy shows room-temperature (RT) superplasticity, and Alhamidi et al. [18] found that as-HPT Al–30 mol%Zn alloy shows annealing hardening.

Although as-HPT Al–Zn alloys have received much attention, application as structural materials of these alloys is limited because of their low strength. The yield strength of as-HPT Al–30 wt%Zn alloy is as low as 50 MPa, which is almost equivalent to the yield strength of pure Al [16]. Although as-HPT Al–Zn alloys show annealing hardening, their yield strength is still very low after annealing, which does not exceed 100 MPa [18].

In our prior work, cold rolling was performed on as-SS Al–Zn alloy [21]. We found that the hardness of the as-rolled Al–Zn alloy after application of 90% rolling reduction ratio (the equivalent plastic strain is about 2.9) was nearly one time higher than that of the as-SS sample. Different from the as-HPT Al–Zn samples, the as-rolled Al–Zn alloy was characterized by high density of dislocations, high Al matrix solubility, high density of nanosized Zn precipitates, and large number of subgrains. The strengthening mechanism of this alloy includes precipitation strengthening, work hardening, solid-solution strengthening, and GB hardening. Therefore, the Al–Zn alloys under a small degree of deformation may have strong application potential in structural materials.

Artificial aging treatment is an effective method to improve the ductility of metals. In the present study, the Al–Zn alloy after

* Corresponding author.
*E-mail address:* zyma@imr.ac.cn (Z.Y. Ma).

http://dx.doi.org/10.1016/j.msea.2016.01.079
0921-5093/

application of 2.9 rolling strain, which shows the highest hardness in as-deformed Al–Zn alloy [21], was artificially aged under different conditions to prepare Al–Zn alloys with high strength and high ductility. The strengthening and deformation mechanisms of the as-rolled and as-aged Al–Zn alloys were also analyzed.

## 2. Experimental methods

Al–20 wt% Zn alloy was prepared by melting high-purity components in vacuum. The castings were cut into samples with dimensions of 16 mm × 80 mm × 200 mm, solution-treated at 550 °C for 3 h, and quenched in water. The samples were then rolled from 16 mm to 1.3 mm for 10 cycles at RT (the plastic strain is about 2.9) at a rolling speed of 0.5 m/s. The as-rolled Al–20 wt% Zn samples were artificially aged at 70–200 °C for 15–960 min, followed by air cooling to RT.

The microstructures were examined using optical microscopy (OM) and transmission electron microscopy (TEM). OM images were taken from rolling direction–normal direction planes, and TEM images were taken from rolling direction–transverse direction planes. Tensile specimens were machined with the tensile axis parallel to the rolling direction. Tensile tests were performed at a strain rate of $1 \times 10^{-4}\ s^{-1}$ by using an Instron-5982-type test machine. The tests were repeated three times to confirm the reproducibility and reliability of the results.

## 3. Results

The OM images of the Al–20 wt% Zn alloys fabricated by different processes are shown in Fig. 1. Equiaxed grains with an average size of approximately 200 μm were obtained in the as-SS sample (Fig. 1a). By comparison, the grains of the as-rolled Al–20 wt% Zn alloy were significantly elongated along the rolling direction, with shear bands at 45° angles with respect to the rolling direction (Fig. 1b). When the rolled Al–20 wt% Zn alloy was aged at 100 °C for 960 min, no significant changes were observed under OM, as shown in Fig. 1c. After aging at 200 °C for 600 min, while the thickness of the elongated grains in the as-rolled sample slightly increased, the shear bands still remained (Fig. 1d).

Fig. 2 shows the TEM images of the as-SS and as-rolled Al–20 wt% Zn alloys. The microstructure of the as-SS sample was characterized by low density of dislocations, well-defined GBs, and absence of precipitates (Fig. 2a). After application of 2.9 rolling strain, the subgrain boundaries (SBs) were obtained in the elongated grains (Fig. 2b). The GBs in the as-rolled sample are often designated as 'non-equilibrium GBs' because these GBs contain large number of dislocations. Furthermore, high density of dispersoids with an equiaxed shape and a size of below 50 nm were also observed in the as-rolled Al–20 wt% Zn alloy, as shown in Fig. 2c.

Fig. 3 shows the TEM images of Al–20 wt% Zn alloys aged at 70 °C for different times. After 60 min aging, the grain structure of the sample did not significantly change (Fig. 3a). When the aging time was increased to 240 min, the recrystallized grains (RX-grains) with an equiaxed shape were produced, and a large number of dislocations still remained in the grain interiors and at GBs (Fig. 3b). Furthermore, the dispersoids coarsened to approximately 100 nm after aging for 240 min (Fig. 2c).

Fig. 4 shows the TEM images of Al–20 wt% Zn samples aged at 100 °C for different times. Aging at 100 °C for 120 min led to the appearance of RX-grains in the Al–20 wt% Zn samples (Fig. 4a and c), and the size and structure of the RX-grains were similar to

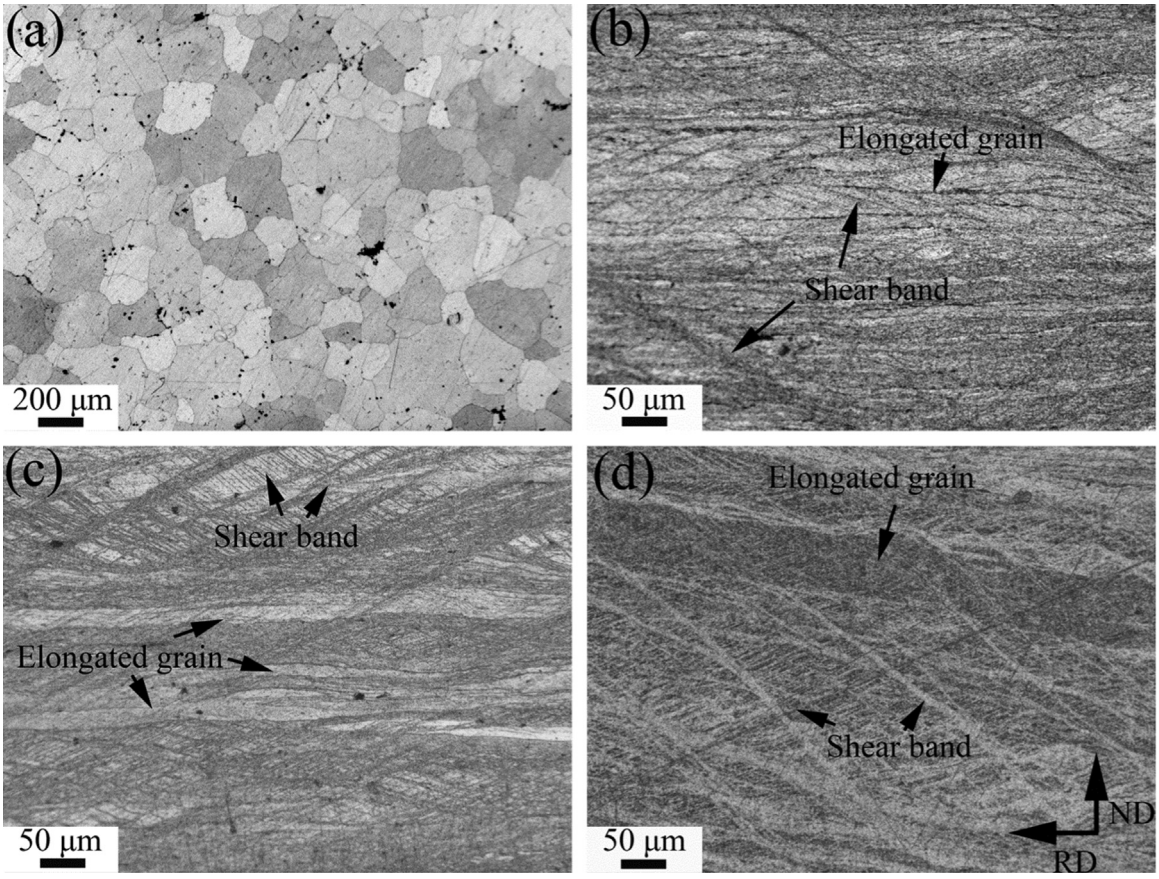


**Fig. 1.** OM images of (a) as-SS, (b) as-rolled, and as-aged Al–20 wt% Zn Alloy performed at (c) 100 °C for 960 min and (d) 200 °C for 600 min.

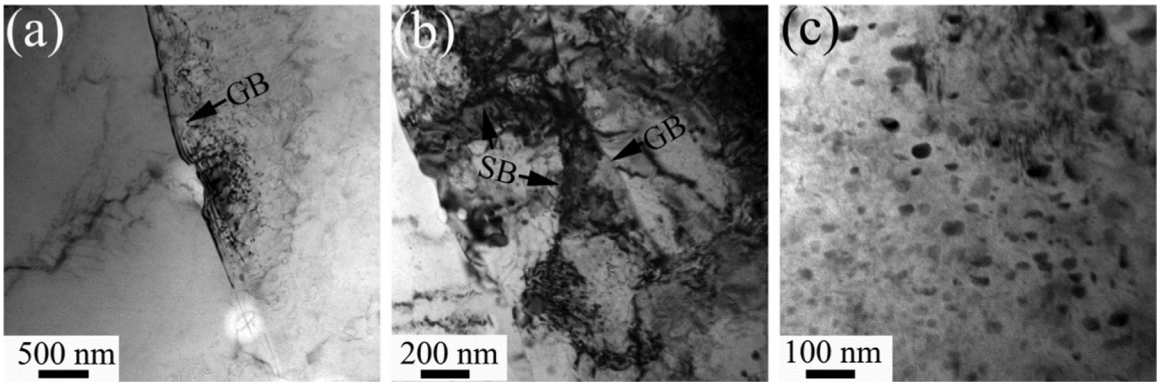


**Fig. 2.** TEM images of (a) as-SS, (b) and (c) as-rolled Al–20 wt% Zn alloy.

those of the sample aged at 70 °C for 240 min. Upon further increasing the aging time to 960 min, the non-equilibrium GBs changed to well-defined GBs, and dislocation free grains were obtained (Fig. 4e). The 960 min-aged sample also showed low density of dislocations.

Fig. 4b, d, and f show the evolution process of Zn precipitation during aging at 100 °C. Aside from equiaxed shaped dispersoids that precipitated during rolling, rod-like dispersoids were also observed in the Al–20 wt% Zn alloy after aging for 30 min. With the increase in aging time, the proportion and average size of the equiaxed dispersoids increased.

Fig. 5 shows the TEM images of the rolled Al–20 wt% Zn samples aged at 200 °C for different times. After 15 min of aging, recrystallization occurred, and the density of dislocations slightly decreased (Fig. 5a). Furthermore, a large number of rod-like dispersoids precipitated in the Al matrix after 15 min of aging, and the average size of precipitates was approximately 30 nm (Fig. 5b), which is less than that of the equiaxed dispersoids in the as-rolled sample. The high-resolution TEM image shows that thin layers of precipitated Zn phase developed between the Al grains and the thickness of the layers was approximately 1.5 nm, as shown in Fig. 5c.

After aging at 200 °C for 60 min, equiaxed RX-grains with a size of approximately 500 nm were obtained (Fig. 5d). The grains of the Al matrix had considerably low dislocation density. Some precipitates measured 100–200 nm in size were located at the triple junctions of the Al grains, as shown in Fig. 5d. Furthermore, the precipitates measured below 70 nm in size were observed within the Al grains (Fig. 5e). Fig. 5f shows that the thickness of the precipitation phase layers between the Al grains in the 60 min-aged sample reached 13 nm.

Upon further increasing aging time to 600 min, the grain size of the Al matrix obviously coarsened, larger than 1 μm, as shown in Fig. 5g. Fig. 5h and i show the bright-field and dark-field (DF) images of the GBs in the 600 min-aged sample, respectively. The DF image, excited using the reflection of Zn phase, clearly showed that the thickness of Zn layers between the Al grains was 25 nm.

The stress–strain curves of the as-SS and as-rolled Al–20 wt% Zn alloys are compared in Fig. 6. After application of 2.9 rolling strain, the ultimate strength (UTS), 0.2% yield strength (YS), and total elongation (EL) of the sample simultaneously increased and reached 350 MPa, 257 MPa, and 11.1%, respectively. Compared with the as-SS sample, the as-rolled Al–20 wt% Zn alloy showed low work-hardening capability.

Fig. 7 shows the stress–strain curves of the as-aged Al–20 wt% Zn alloys under different aging conditions. The samples aged at 70 °C showed good mechanical stability, and extending the aging time from 60 to 240 min only led to a slight decrease in YS and EL, but nearly invariant UTS. For 100 °C aging, both the strength and ductility of the Al–20 wt% Zn alloys deteriorated with increasing aging time. However, the EL of the sample aged for a short duration of 30 min exhibited an increase (13%) compared to the as-rolled sample. Aging at 200 °C resulted in significantly reduced strength and much improved ductility. As the aging time increases the strength and ductility decreased and the best mechanical properties were achieved after 15 min of short-duration aging, with the EL being 22%, YS and UTS being 194 MPa and 280 MPa, respectively.

## 4. Discussion

### 4.1. Recrystallization

The as-rolled Al–20 wt% Zn alloy showed a typical deformation microstructure, namely, elongated Al grains, high density of

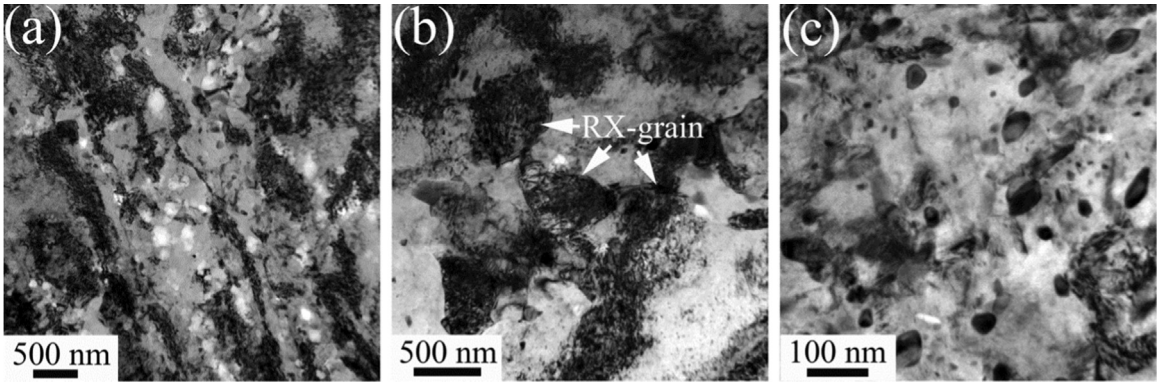


**Fig. 3.** TEM images of as-aged Al–20 wt% Zn alloy performed at 70 °C for (a) 60 min (b) and (c) 240 min.

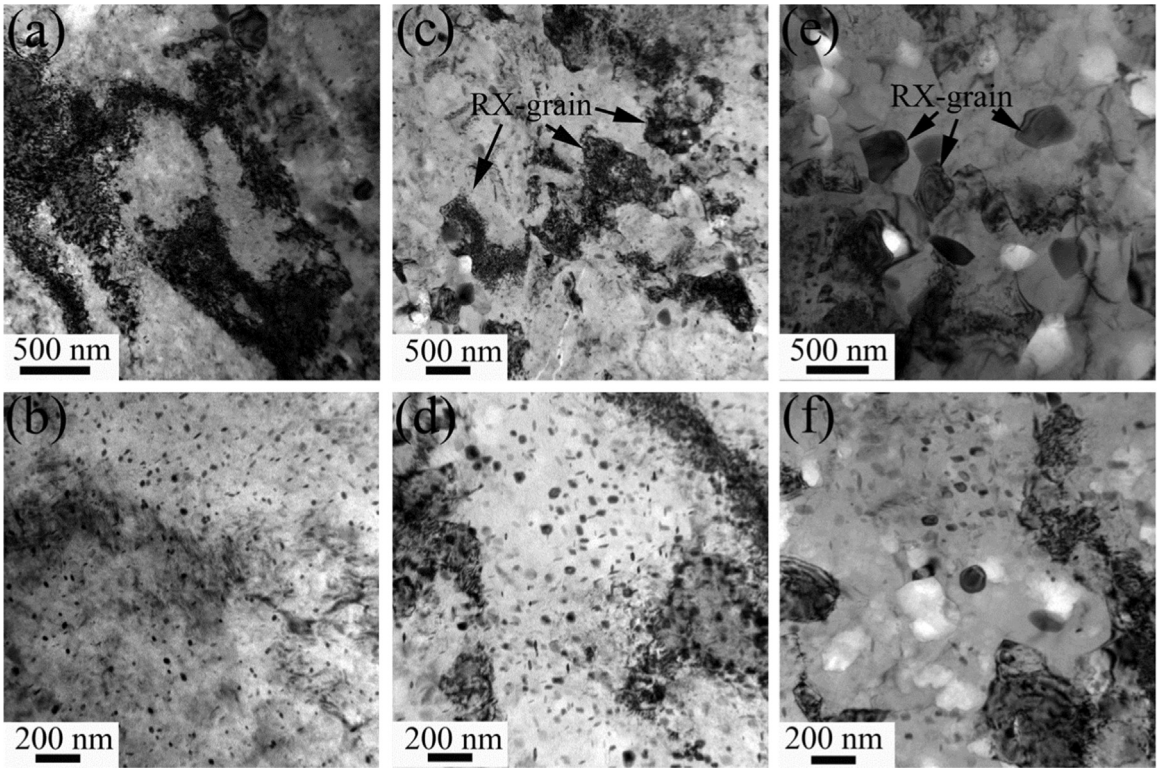


**Fig. 4.** TEM images of as-aged Al–20 wt% Zn alloy performed at 100 °C for (a) and (b) 30 min, (c) and (d) 120 min, and (e) and (f) 960 min.

dislocations, and shear bands. The elongated grains showed high thermal stability below 200 °C, as shown in Fig. 1. Meanwhile, equiaxed RX-grains with a size of hundreds of nanometers were also obtained in the samples after long-period or high temperature aging (Figs. 3b, 4e, 5d and g). Then, a bimodal structure containing ultra-fine and elongated grains was observed in the as-aged Al–20 wt% Zn alloys.

In the as-rolled Al–20 wt% Zn alloy, the density of dislocations in the shear bands was higher than that in other regions. The dislocations have a significant contribution to the stored energy, which is the driving force for both recovery and recrystallization [22]. Thus, recrystallization occurred preferentially in the shear bands of the as-rolled samples during aging treatment, and was completed after aging at 100 °C for 960 min or 200 °C for 60 min as shown in Figs. 4e and 5d. The aging conditions in the present study did not lead to disappearance of elongated grains, but greatly reduced the density of dislocations because of annealing recovery.

### 4.2. Precipitation

The precipitation phase, as well as typical deformation microstructure, was obtained in the as-rolled Al–20 wt% Zn alloy. Our previous study showed the formation of Zn clusters during RT rolling under a very small degree of deformation. With the increase in rolling deformation, the evolution process of Zn phase is as follows: cluster→rod-like phase→equiaxed phase→phase coarsening [21]. The equiaxed Zn phase was obtained after application of 2.9 rolling strain (Fig. 2c). The 70 °C aging led to the coarsening of Zn phase, while both phase coarsening and formation of new Zn phase occurred during aging at higher temperatures (Figs. 3–5).

A large number of dislocations were observed near the nanosized precipitate/matrix interfaces after rolling [21]. These dislocations provided the driving force for the Zn precipitation and led to the coarsening of the original Zn phase during low temperature aging (Fig. 3c). Clearly, the new Zn phase precipitation needs more energy. RT rolling leads to the formation of large number of vacancies that are ideal sites for precipitation of solute atoms. Therefore, a large number of rod-like dispersoids precipitated in the Al matrix after a short period of aging at 100 and 200 °C (Figs. 4b and 5b). With the increase in aging time, the rod-like dispersoids changed to equiaxed shape and then coarsened, and were finally located at the triple junctions of the Al grains (Figs. 4d, 4f, 5d and 5e). The evolution process of Zn precipitation during aging was similar to that of dynamic precipitation [14–21].

The GBs in the as-rolled Al–20 wt% Zn alloys contain a large number of dislocations (non-equilibrium GBs). The high density of dislocations provided a large number of atom propagation channels, thereby enhancing the mobility of Zn atoms during aging. Thus, the Zn atoms tended to gather in the GBs, and the Zn phase layers formed during aging. A very thin Zn layers with a thickness of several nanometers can be identified between the Al grains after aging at 200 °C for 15 min (Fig. 5c). With increasing aging time, the thickness of the Zn layers increased, and the non-equilibrium GBs changed to equilibrium GBs (Fig. 5f and i). The formation of Zn phase layers between the Al grains were also observed in the Al–20 wt% Zn alloys after severe plastic deformation such as HPT [16,20].

### 4.3. Strengthening and deformation mechanisms

Fig. 8 summarizes the tensile properties of the Al–Zn alloys based on the present study and previous reports. Compared with as-HPT Al–Zn alloys, the as-rolled and as-aged Al–Zn alloys showed higher strength but lower EL, although these samples contained less Zn.

For the as-rolled Al–20 wt% Zn alloy, the main strengthening mechanisms include precipitation strengthening by nanosized Zn precipitates, work hardening by dislocations, and solid-solution strengthening by lattice distortion. The net effects led to high strength in the as-rolled sample. After aging, the density of

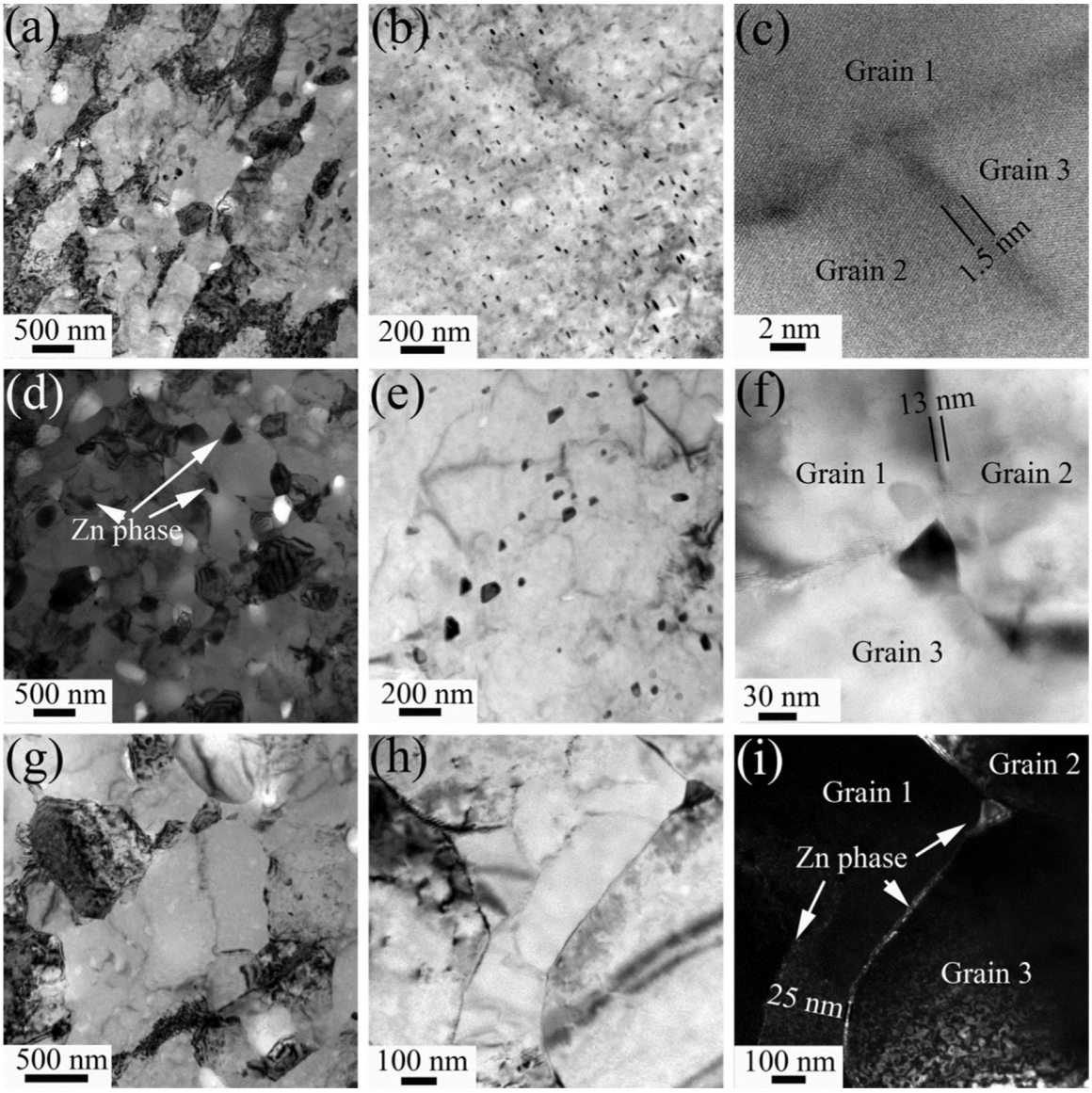


**Fig. 5.** TEM images of as-aged Al–20 wt% Zn alloy performed at 200 °C for (a), (b), and (c) 15 min; (d), (e), and (f) 60 min; and (g), (h), and (i) 600 min.

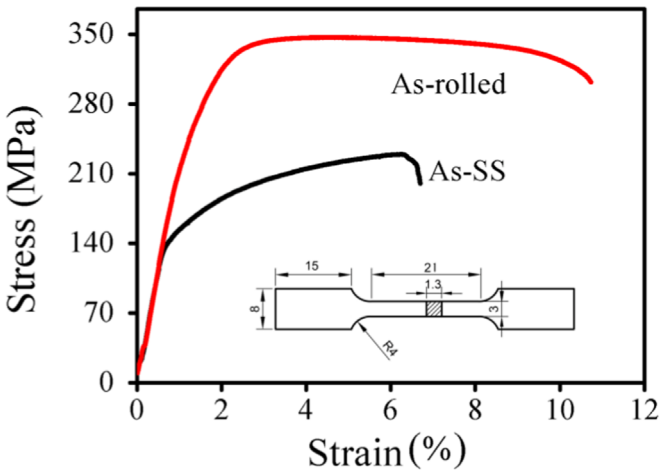


**Fig. 6.** Stress–strain curves of as-SS and as-rolled Al–20 wt% Zn alloys. The inset shows the dimension of the tensile specimens.

dislocations in the Al–20 wt% Zn alloys decreased, the density and size of the Zn precipitate increased, and the Zn solubility decreased in the Al lattice. Thus, the YS of the as-aged Al–20 wt% Zn alloys were lower than that of the as-rolled sample.

The stress–strain curve of the as-rolled Al–20 wt% Zn alloy showed obvious work softening after yielding (Fig. 6). Two competitive processes occurred during tension: (i) the increase of dislocation density led to work hardening, and (ii) annihilation and rearrangement of the preexisting dislocations led to work softening. The extent to which the two processes occurred directly depends on the preexisting dislocation density [23]. The high density of dislocations in the as-rolled Al–20 wt% Zn alloy led to that the latter process overrides the former, and consequently, work softening occurs in the sample. Aging treatment effectively decreases the density of dislocations, and then increases the work hardening rate of Al–20 wt% Zn alloy. Compared with the as-rolled Al–20 wt% Zn alloy, the 70 °C-aged sample shows higher UTS and EL because of higher work hardening rate (Fig. 7a).

The EL of 100 °C-aged Al–20 wt% Zn alloys decreased with the increase in aging time from 30 to 960 min as shown in Fig. 7b. The

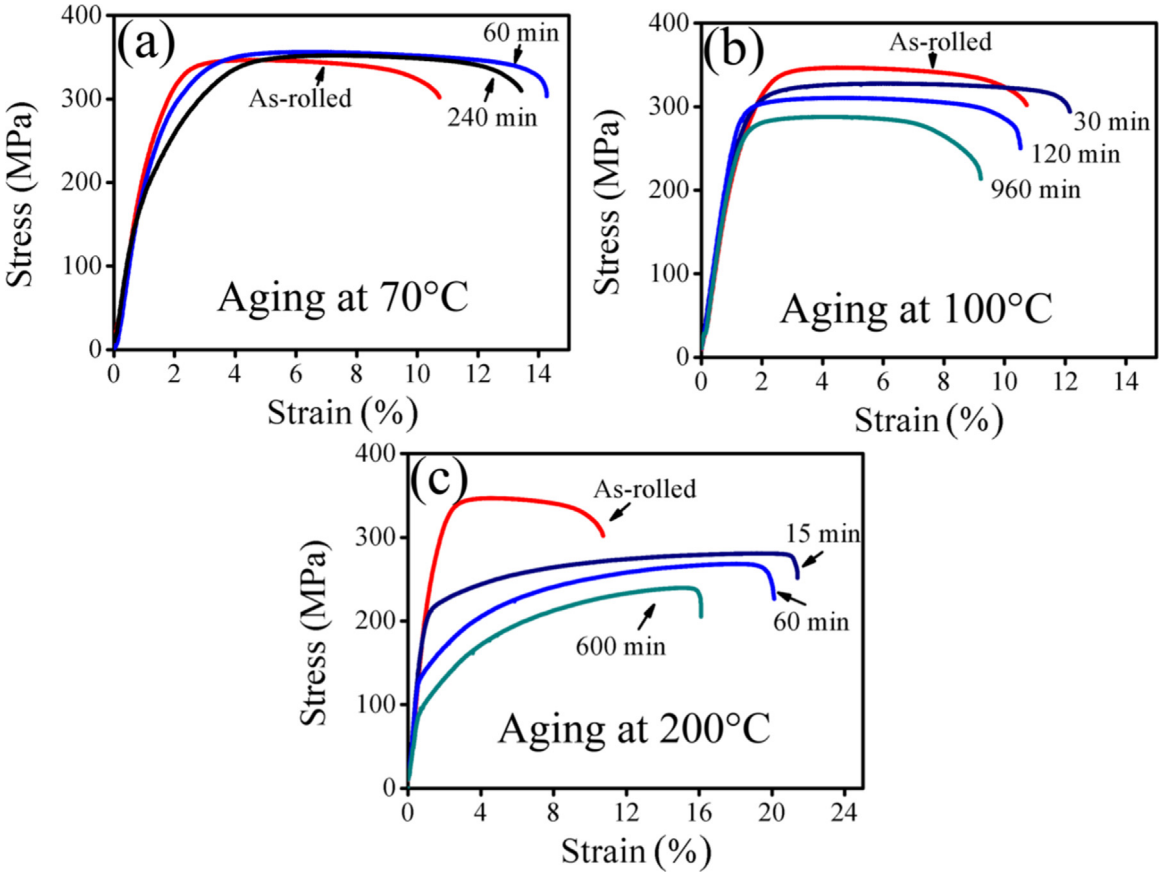


**Fig. 7.** Stress–strain curves of as-aged Al–20 wt% Zn alloys performed at (a) 70 °C, (b) 100 °C, and (c) 200 °C.

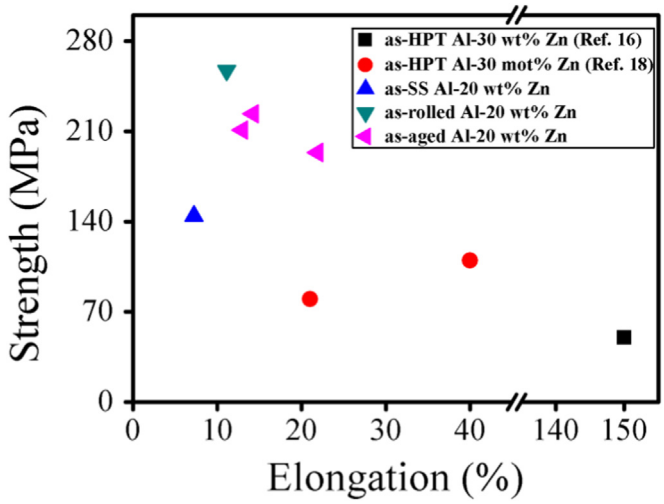


**Fig. 8.** Summary of the tensile properties of Al–Zn alloys from the literatures and this study.

Zn phase coarsened with the aging time and acted as preferential sites for crack nucleation during the tensile process. Then, the plastic instability and the onset of necking occurred in the as-aged Al–20 wt% Zn alloys after aging at 100 °C for 960 min.

The trend in the change of EL during 200 °C aging is similar to that during 100 °C (Fig. 7c). Peak value appeared at short aging period. The EL of 200 °C-15 min-aged Al–20 wt% Zn alloy is one time higher than that of the as-rolled sample. The bimodal structures of Al alloys composed of fine grains and elongated coarse grains often show high ductility and strength [24–26]. Bimodal structures were also obtained in the 200 °C-aged Al–20 wt% Zn alloys as shown in Figs. 1d, 5a, 5d and 5g. The coarse grains with high dislocation absorption capacity can effectively impede the propagation of microcracks during tension. Fine grains enhance the strength through the Hall–Petch relationship. Therefore, the 200 °C-aged Al–20 wt% Zn alloys shows enhanced ductility while retaining high strength.

Valiev et al. [16] demonstrated that the as-HPT Al–30 wt% Zn alloy showed RT superplasticity (150%). The reason for this phenomenon can be attributed to the development of thin layers of Zn-rich GB phases, which leads to the occurrence of enhanced Al GB sliding. In this study, the thin Zn layers with several nanometers were also obtained between Al grains after aging at 200 °C for 15 min (Fig. 5c). Thus, the Zn layers also played a significant role at the high EL of 200 °C-15 min-aged Al–20 wt% Zn alloy. With the increase in aging time, the thickness of the Zn layers increased, reducing the Al GB sliding capacity. The interface between the Zn layers and Al GBs also provided a preferential crack propagation path, leading to the decrease in EL.

## 5. Conclusions

This study suggests the potential for achieving high strength and high ductility in binary Al–Zn alloys using rolling and aging treatments. The following conclusions are reached:

(1) The recrystallization occurred preferentially in the shear bands of the as-rolled Al–20 wt% Zn alloy during aging treatment, and was completed after aging at 100 °C for 960 min or 200 °C for 60 min. The elongated grains in the as-rolled Al–20 wt% Zn alloy show high thermal stability below 200 °C. A bimodal structure containing ultra-fine and elongated coarse

grains was formed in the as-aged Al–20 wt% Zn alloys.
(2) The Zn phase precipitated from Al lattice in Al–20 wt% Zn alloy after an application of 2.9 rolling strain. The formation of Zn layers between Al grains as well as the coarsening of original Zn phase and the precipitation of new Zn phase occurred in the as-rolled Al–20 wt% Zn alloy during the subsequent aging.
(3) The as-rolled Al–20 wt% Zn alloy showed high strength (YS and UTS being 257 MPa and 350 MPa, respectively). Aging at 60–200 °C for short periods, the as-aged Al–20 wt% Zn alloys showed balanced mechanical properties, including enhanced ductility, and reasonable strength, compared with the as-rolled sample.
(4) The bimodal structure and thin Zn layers, caused by recrystallization and precipitation, respectively, during aging, played significant roles in determining the mechanical properties of as-aged Al–20 wt% Zn alloys.

## Acknowledgments

This work was funded by the National Basic Research Program of China (No. 2013CB733000), Guangxi Natural Science Foundation (No.2015GXNSFBA139238), and the Guangxi 'Bagui' Teams for Innovation and Research.

## References

[1] R. Valiev, Nat. Mater. 3 (2004) 511–516.
[2] P.V. Liddicoat, X.Z. Liao, Y.H. Zhao, Y.T. Zhu, M.Y. Murashkin, E.J. Lavernia, R. Z. Valiev, S.P. Ringer, Nat. Commun. 1 (2010) 63–69.
[3] G. Sha, K. Tugcu, X.Z. Liao, P.W. Trimby, M.Y. Murashkin, R.Z. Valiev, S.P. Ringer, Acta Mater. 63 (2014) 169–179.
[4] I. Sabirov, M.Yu Murashkin, R.Z. Valiev, Mater. Sci. Eng. A 560 (2013) 1–24.
[5] W. Chrominski, M. Kulczyk, M. Lewandowska, K.J. Kurzydlowski, Mater. Sci. Eng. A609 (2014) 80–87.
[6] W.Z. Han, Z.F. Zhang, S.D. Wu, S.X. Li, Y.D. Wang, Philos. Mag. Lett. 86 (2006) 435–441.
[7] Y.H. Zhao, X.Z. Liao, S. Cheng, E. Ma, Y.T. Zhu, Adv. Mater. 18 (2006) 2280–2283.
[8] C.Y. Liu, P.F. Yu, X.Y. Wang, M.Z. Ma, R.P. Liu, Int. J. Min. Met. Mater. 21 (2014) 702–710.
[9] Y. Saito, N. Tsuji, H. Utsunomiya, T. Sakai, R.G. Hong, Scr. Mater. 39 (1998) 1221–1227.
[10] X.X. Huang, Scr. Mater. 60 (2009) 1078–1082.
[11] Z.Y. Ma, Metall. Mater. Trans. A 39 (2008) 642–658.
[12] P. Xue, B.L. Xiao, Z.Y. Ma, J. Mater. Sci. Technol. 29 (2013) 1111–1115.
[13] P. Xue, B.L. Xiao, Z.Y. Ma, Acta Metal. Sin. 50 (2014) 245–251.
[14] B. Straumal, B. Baretzky, A. Mazilkin, F. Phillipp, O. Kogtenkova, M. Volkov, R. Valiev, Acta Mater. 52 (2004) 4469–4478.
[15] A.A. Mazilkin, B.B. Straumal, E. Rabkin, B. Baretzky, S. Enders, S.G. Protasova, O. A. Kogtenkova, R.Z. Valiev, Acta Mater. 54 (2006) 3933–3939.
[16] R.Z. Valiev, M.Y. Murashkin, A. Kilmametov, B. Straumal, N.Q. Chinh, T. G. Langdon, J. Mater. Sci. 45 (2010) 4718–4724.
[17] N.Q. Chinh, T. Csanadi, T. Győri, R.Z. Valiev, B.B. Straumal, M. Kawasaki, T. G. Langdon, Mater. Sci. Eng. A 543 (2012) 117–120.
[18] A. Alhamidi, K. Edalati, Z. Horita, S. Hirosawa, K. Matsuda, D. Terada, Mater. Sci. Eng. A 610 (2014) 17–27.
[19] M. Borodachenkova, F. Barlat, W. Wen, A. Bastos, J.J. Grácio, Int. J. Plasticity 68 (2015) 150–163.
[20] X. Sauvage, M.Y. Murashkin, B.B. Straumal, E.V. Bobruk, R.Z. Valiev, Adv. Eng. Mater. 17 (2015) 1821–1827.
[21] C.Y. Liu, L. Yu, M.Z. Ma, R.P. Liu, Z.Y. Ma, Phil. Mag. Lett. 95 (2015) 539–546.
[22] N. Kamikawa, X.X. Huang, N. Hansen, J. Mater. Sci. 43 (2008) 7313–7319.
[23] Y.J. Lin, Y.G. Zhang, B.Q. Xiong, E.J. Lavernia, Mater. Lett. 82 (2012) 233–236.
[24] D. Witkin, Z. Lee, R. Rodriguez, S. Nutt, E.J. Lavernia, Scr. Mater. 49 (2003) 297–302.
[25] Z. Lee, V. Radmilovic, B. Ahn, E.J. Lavernia, S.R. Nutt, Metall. Mater. Trans. A 41 (2010) 795–801.
[26] B.Q. Han, J.Y. Huang, Y.T. Zhu, E.J. Lavernia, Acta Mater. 54 (2006) 3015–3024.